Journal of Materials Chemistry A

ROYAL SOCIETY OF CHEMISTRY

PAPER

View Article Online
View Journal | View Issue

Cite this: J. Mater. Chem. A, 2025, 13, 12482

A computational view on the thermochemical and electrochemical stability of ruthenium oxides†

Iratxe Aguado-Ruiz, ‡[ab] Ricardo Urrego-Ortiz ‡[ab] and Federico Calle-Vallejo *[bc]

Received 27th December 2024
Accepted 17th March 2025

DOI: 10.1039/d4ta09213a

rsc.li/materials-a

Ruthenium oxides (RuO_x) display suitable activities for a number of electrocatalytic reactions, such as chlorine evolution and oxygen evolution. However, their corrosion resistance still ought to be enhanced and the instabilities are often attributed to the transformation of one Ru oxide into another. Density functional theory (DFT) calculations can help understand and improve the thermochemical and electrochemical stability of RuO_x. However, in this work, we show that a wide variety of exchange-correlation functionals are visibly inaccurate for the thermochemistry of gas-phase and solid-state RuO_x. The inaccuracies can be systematically mitigated, as they grow alongside the number of oxygen atoms in the compounds because of the repulsive interactions among Ru–O bonds. Furthermore, Pourbaix diagrams, which are electrochemical phase diagrams outlining the conditions of electrode stability, are shown to be significantly affected by these inaccuracies. Seamlessly, our simple correction scheme brings computational Pourbaix diagrams close to experimental results, giving confidence in the predictiveness of future stability studies.

1. Introduction

Ruthenium oxides (RuO_x, $x = 1$–4) are a family of chemical compounds in which the metal atom displays a wide range of oxidation states, from +2 in RuO to +8 in RuO_4. These oxides are relevant in diverse branches of chemistry, from nuclear energy to heterogeneous catalysis and electrochemistry.[1–3] Among them, ruthenium dioxide (RuO_2) is of particular importance due to its activity to electrocatalyze the chlorine and oxygen evolution reactions (CER and OER, respectively),[4–8] the former being central in the chloralkali process, the latter in water electrolyzers, and both in competition during seawater electrolysis.[9,10] In addition, RuO_2 also helps catalyze the thermocatalytic Sumitomo process, in which HCl is oxidized to Cl_2.[3,11] In all these applications, efficient use of RuO_x-based materials is crucial, as ruthenium is not particularly abundant in the Earth's crust,[12] the chloralkali electrolysis is a notorious and energy-intensive industrial process, and water electrolyzers are key for producing green hydrogen.

Consequently, efforts have been directed to investigate the factors governing the catalytic performance of RuO_2, such as facet orientation,[13] ligand effects,[14] crystal structure,[15] and doping.[16,17] However, the chemical and structural features of RuO_2 are interconnected in such a way that disclosing their effects on the catalytic activity is challenging from an experimental standpoint. Density functional theory (DFT) calculations coupled with thermodynamic models are valuable tools to address this matter, as they can be used to estimate the energies of reaction intermediates under different conditions, thus serving as a guide, support and supplement to experiments.[17–20]

In this context, it is paramount to properly assess the accuracy of DFT-calculated thermochemistry. In particular, the formation energies of oxides, gas-phase species, and OER intermediates have proved challenging for DFT,[21–28] leading to inaccurate reaction energies, equilibrium potentials and adsorption energies that deviate from experimental observations.[29,30] In addition, incorrect thermochemical predictions might lead to incorrect assessments of the stability of Ru-based electrodes, which are critical to ensure their suitability as catalysts, elucidate the state of the active sites under reaction conditions, and guarantee their durability.[31–34] This calls for strategies that can swiftly pinpoint and rectify inaccurate results at the early stages of computational studies on these compounds.

In this work, we evaluate the DFT formation energies of several RuO_x using exchange-correlation functionals of increasing

[a]Department of Materials Science and Chemical Physics, Institute of Theoretical and Computational Chemistry (IQTCUB), University of Barcelona, C/Martí i Franquès 1, 08028 Barcelona, Spain

[b]Nano-Bio Spectroscopy Group, European Theoretical Spectroscopy Facility (ETSF), Department of Advanced Materials and Polymers: Physics, Chemistry and Technology, University of the Basque Country UPV/EHU, Av. Tolosa 72, 20018 San Sebastián, Spain. E-mail: federico.calle@ehu.es

[c]Ikerbasque, Basque Foundation for Science, Plaza de Euskadi 5, 48009 Bilbao, Spain

† Electronic supplementary information (ESI) available. See DOI: https://doi.org/10.1039/d4ta09213a

‡ These authors contributed equally to this work.

complexity (GGAs, meta-GGAs, and hybrids) to evaluate if systematic errors exist and whether more sophisticated functionals necessarily lead to enhanced thermochemical predictions of Ru oxides. We unveil large errors that scale linearly with the number of oxygen atoms of the oxides and systematically prevent accurate thermochemical predictions. Moreover, we provide a simple but insightful model to rationalize this intriguing trend. Finally, by means of Pourbaix diagrams[35] of the Ru–water system, we show the detrimental effects these errors have on electrochemical stability predictions and provide a handy procedure to align the DFT energies with experimental values.

2. Methodology

2.1 Computational methods

The total energies of the Ru-based species ($Ru_{(g)}$, $Ru_{(s)}$, $RuO_{(g)}$, $RuO_{2(g)}$, $RuO_{2(s)}$, $RuO_{3(g)}$ and $RuO_{4(g)}$) in Fig. 1 were obtained with the Vienna *Ab initio* Simulation Package (VASP)[36] using the Projector Augmented-Wave (PAW) method to describe ion–electron interactions.[37] For that, we used three functionals at the level of the generalized gradient approximation (GGA): PBE,[38] PW91,[39] and RPBE;[40] three meta-GGAs:[41] SCAN,[42] TPSS,[43] and R2SCAN;[44] and three hybrid functionals: PBE0,[45] HSEsol,[46] and HSE06.[47]

All atoms in the compounds were allowed to relax in all directions until all the residual forces on them were below 0.01 eV $Å^{-1}$. The reciprocal space was sampled using Monkhorst–Pack grids[48] and only the Γ-point was considered for the molecules. Gaussian smearing was used at an electronic temperature of 0.001 eV to facilitate the convergence of the self-consistent cycles and all energies were extrapolated to 0 K. Spin unrestricted calculations were performed when necessary, namely for $O_{2(g)}$, $Ru_{(g)}$, and $RuO_{(g)}$. The molecules were simulated in cells of 15.00 Å × 15.10 Å × 15.20 Å, which ensured no interaction between the periodically repeated images.

$Ru_{(s)}$ was modelled in its hexagonal close-packed (hcp) structure while $RuO_{2(s)}$ was simulated in its rutile form. For the bulk calculations, all atoms were free to relax in all directions until all residual forces were below 0.05 eV $Å^{-1}$. Test calculations using a tighter force criterion (0.01 eV $Å^{-1}$) showed total energy differences for $Ru_{(s)}$ and $RuO_{2(s)}$ smaller than 0.0001 eV. The smearing was made using the Methfessel–Paxton method[49] at an electronic temperature of 0.2 eV and all energies were subsequently extrapolated to 0 K. Based on the convergence test in Section S7,† we used a plane-wave energy cutoff of 450 eV for all calculations of molecules and solids.

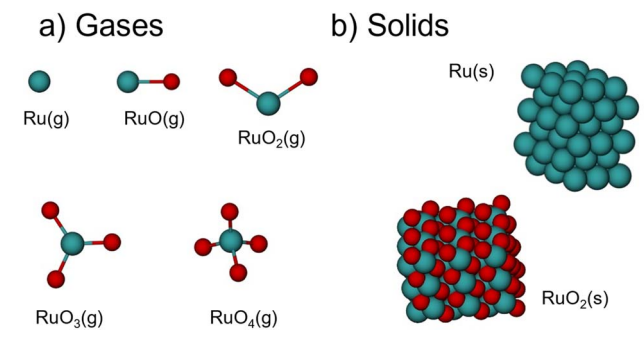

Fig. 1 Schematics of (a) the gas-phase species and (b) the solids analyzed in this work. Green spheres represent ruthenium, and oxygen atoms are shown in red.

2.2 Thermochemical calculations

The formation reaction of the compounds under study is defined in eqn (1), where all species are in their standard states and $x = \{0, 1, 2, 3, 4\}$.

$$Ru_{(s)} + \frac{x}{2}O_{2(g)} \rightarrow RuO_x \quad (1)$$

The free energy of formation for each compound ($\Delta_f G^{XC}_{RuO_x}$) can be approximated using DFT-calculated data as follows:

$$\Delta_f G^{XC}_{RuO_x} \approx \Delta_f E^{XC} + \Delta_f ZPE^{XC} - T\Delta_f S \quad (2)$$

where $\Delta_f E^{XC}$ is the difference between the ground-state energies of the products and reactants considering the stoichiometric coefficients calculated with a given (XC) functional, and $\Delta_f ZPE^{XC}$ is the respective difference of zero-point energies calculated on the basis of DFT vibrational frequencies using the harmonic oscillator approximation. Finally, the term $T\Delta_f S$ is an entropic correction and the individual standard entropies of the reactants and products are retrieved from thermodynamic tables at $T = 298.15$ K.[50–53]

2.3 Evaluating DFT errors

For a given compound RuO_x, the deviation between the experimental ($\Delta_f G^{exp}_{RuO_x}$) and DFT formation energies computed with a particular functional ($\Delta_f G^{XC}_{RuO_x}$) corresponds to the total error $\varepsilon^{T,XC}_{RuO_x}$. Importantly, $\varepsilon^{T,XC}_{RuO_x}$ includes the errors in RuO_x ($\varepsilon^{XC}_{RuO_x}$) and in the reactants of eqn (1) ($\varepsilon^{XC}_{Ru_{(s)}}$ and $\varepsilon^{XC}_{O_2}$), as shown in eqn (3).[27,54–57]

$$\varepsilon^{T,XC}_{RuO_x} = \Delta_f G^{XC}_{RuO_x} - \Delta_f G^{exp}_{RuO_x} = \varepsilon^{XC}_{RuO_x} - \left(\varepsilon^{XC}_{Ru_{(s)}} + \frac{x}{2}\varepsilon^{XC}_{O_{2(g)}}\right) \quad (3)$$

In particular, the triplet state of $O_{2(g)}$ is commonly miscalculated by DFT, yielding substantial $\varepsilon^{XC}_{O_2}$ values.[21,25,58,59] Furthermore, previous studies have unveiled DFT errors above 0.5 eV in oxygen-containing gaseous species,[60–62] such that large values of $\varepsilon^{XC}_{RuO_x}$ are also expected. As GGAs usually describe metals better than molecules,[27] it is customary to assume $\varepsilon^{XC}_{Ru_{(s)}} \approx 0$ as a first approximation, which might be reconsidered for hybrid functionals. Thus, reorganizing eqn (3) we have: $\varepsilon^{XC}_{RuO_x} = \varepsilon^{T,XC}_{RuO_x} + \frac{x}{2}\varepsilon^{XC}_{O_2}$, which indicates that the specific DFT error of each RuO_x can be evaluated once the $O_{2(g)}$ errors are known. In practice, $\varepsilon^{XC}_{O_2}$ is usually calculated semiempirically using the experimental water formation energy $\left(\frac{1}{2}O_2 + H_2 \rightarrow H_2O\right)$.[21,25,26,54,55] The DFT total errors and the individual molecular errors calculated for all functionals in this work are shown in Tables S2 and S3.†

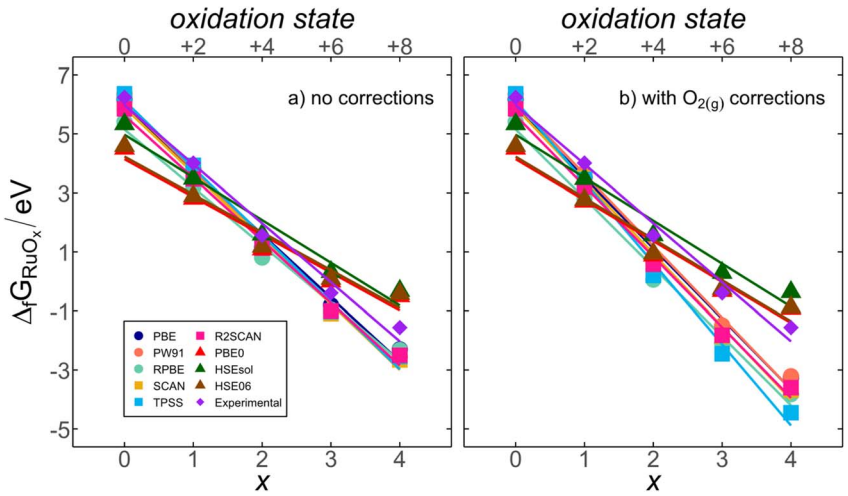

Fig. 2 DFT-calculated formation energies of ruthenium oxides ($\Delta_f G_{RuO_x}$) as a function of the number of oxygen atoms (x) and Ru oxidation state using several functionals when (a) no corrections are included, and (b) the energy of $O_{2(g)}$ is corrected. In both cases, the experimental trend is included. Circles correspond to GGAs, squares to meta-GGAs, triangles to hybrids, and diamonds to the experimental data.

3. Results and discussion

3.1 Energy–structure relationship

Ru displays increasing oxidation states as the number of oxygen atoms in the compound (x) grows from +2 in $RuO_{(g)}$ to +8 in $RuO_{4(g)}$. The experimental and DFT-calculated formation energies, with and without $O_{2(g)}$ corrections, show a strong correlation with x (or the oxidation state of Ru), as shown in Fig. 2. This suggests the existence of a systematic connection between chemical composition and energy for RuO_x. In the following, we provide an energy-decomposition model[63–65] to rationalize the linear relationships in Fig. 2. The model is based on three considerations:

(1) The free energy of eqn (1) is $\Delta_f G_{RuO_x} = G_{RuO_x} - \frac{x}{2}G_{O_2} - G_{Ru_{(s)}}$, and the free energies of the species include their internal energy, ZPE and entropic corrections, in line with eqn (2).

(2) The total energy of the oxide ($E_{RuO_{x(g)}}$) can be decomposed into the sum of the energy of Ru–O bonds plus an interaction energy $E_{int}(x)$ between different Ru–O moieties: $E_{RuO_{x(g)}} = xE_{Ru-O} + E_{int}(x)$. As shown in Table S5,† the energy of the Ru–O bonds in RuO_x can be approximated to the energy of $RuO_{(g)}$. Therefore $E_{RuO_{x(g)}} \approx xE_{RuO(g)} + E_{int}(x)$.

(3) $E_{int}(x)$ is observed in Section S3† to scale linearly with x for all functionals, such that $E(x)_{int} \approx \alpha x + \beta$, where α and β are functional-specific constants.

These three considerations lead to eqn (4):

$$\Delta_f G_{RuO_{x(g)}} \approx \left(E_{RuO_{(g)}} + \alpha - \frac{1}{2}G_{O_2}\right)x + \left(\beta + ZPE_{RuO_x} - TS_{RuO_x} - G_{Ru_{(s)}}\right) \quad (4)$$

When the terms in eqn (4) are calculated using DFT and a specific functional, eqn (5) is obtained, where

$$m^{XC}_{RuO_x} = \left(E^{XC}_{RuO_{(g)}} + \alpha^{XC} - \frac{1}{2}G^{XC}_{O_2}\right) \quad \text{and} \quad b^{XC}_{RuO_x} = \beta^{XC} + ZPE_{RuO_x} - TS_{RuO_x} - G^{XC}_{Ru_{(s)}}.$$

$$\Delta_f G^{XC}_{RuO_{x(g)}} \approx m^{XC}_{RuO_x}x + b^{XC}_{RuO_x} \quad (5)$$

Eqn (5) explains the linear trends in Fig. 2a, in which free energies and oxygen content are shown to vary proportionally. Importantly, $G^{XC}_{O_2}$ is the uncorrected free energy of $O_{2(g)}$. When $O_{2(g)}$ is corrected, $G^{XC}_{O_2}$ is replaced by $G^{XC,OC}_{O_2} = G^{XC}_{O_2} - \varepsilon^{XC}_{O_2}$ ("OC" stands for oxygen corrected), as shown in Fig. 2b. Table S1† shows the experimental and DFT-calculated formation energies obtained using eqn (2), without and with the $O_{2(g)}$ correction ($\Delta_f G^{XC}_{RuO_{x(g)}}$ and $\Delta_f G^{XC,OC}_{RuO_{x(g)}}$, respectively), for all scrutinized functionals. Table S9† contains the parameters of the fits in Fig. 2b and those obtained with the $O_{2(g)}$-corrected version of eqn (5). Section S3† contains further details of the model.

3.2 Trends in the gas-phase errors of RuO_x

The total errors in the DFT-calculated energies of RuO_x ($\varepsilon^{T,XC}_{RuO_x}$) were calculated using eqn (3) for all the examined functionals. Upon correcting $O_{2(g)}$, the individual errors ($\varepsilon^{XC}_{RuO_x}$) were also computed. Both $\varepsilon^{T,XC}_{RuO_x}$ and $\varepsilon^{XC}_{RuO_x}$ scale with the number of oxygen atoms in the oxide, as shown in Fig. 3a and b for the GGAs and meta-GGAs, and in Fig. 3c and d for hybrid functionals, respectively.

Fig. 3 unveils a striking difference between the analyzed functionals: the trends for GGAs and meta-GGAs have negative slopes while those of hybrid functionals display positive slopes. Eqn (5) and the definitions of $\varepsilon^{T,XC}_{RuO_x}$ and $\varepsilon^{XC}_{RuO_x}$ can be used to explain such opposing trends. Specifically, the magnitude and sign of the slopes depend on those in Fig. 2 in the way shown in eqn (6):

$$\varepsilon^{T,XC}_{RuO_x} \approx \left(m^{XC}_{RuO_x} - m^{exp}_{RuO_x}\right)x + \left(b^{XC}_{RuO_x} - b^{exp}_{RuO_x}\right) \quad (6)$$

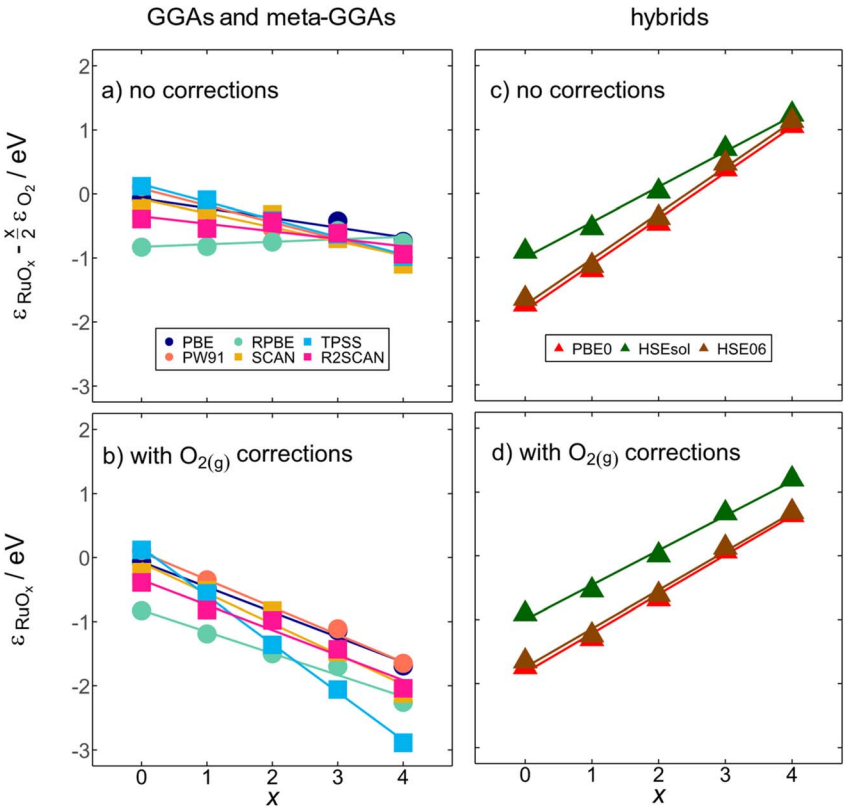

Fig. 3 DFT errors in the formation energies of RuO_x as a function of the number of oxygen atoms (x) in the structure. (a) and (b) are for GGA (circles) and meta-GGA functionals (squares), while (c) and (d) are for hybrid functionals (triangles). The trends in (a) and (c) are for the total errors, that is when no corrections are applied $\left(\varepsilon^{\mathrm{T}} = \varepsilon_{\mathrm{RuO}_x} - \frac{x}{2}\varepsilon_{\mathrm{O}_2}\right)$, while the trends in (b) and (d) correspond to the isolated errors of each oxide ($\varepsilon_{\mathrm{RuO}_x}$), obtained upon correcting $O_{2(g)}$.

Because $m^{\mathrm{XC}}_{\mathrm{RuO}_x}$ and $m^{\mathrm{exp}}_{\mathrm{RuO}_x}$ are negative in Fig. 2, $\varepsilon^{\mathrm{T,XC}}_{\mathrm{RuO}_x}$ scales positively with x when $\left|m^{\mathrm{XC}}_{\mathrm{RuO}_x}\right| < \left|m^{\mathrm{exp}}_{\mathrm{RuO}_x}\right|$ (see Table S9).† Once molecular oxygen has been corrected, we have:

$$\varepsilon^{\mathrm{XC}}_{\mathrm{RuO}_x} = \left(m^{\mathrm{XC}}_{\mathrm{RuO}_x} - m^{\mathrm{exp}}_{\mathrm{RuO}_x} + \frac{1}{2}\varepsilon^{\mathrm{XC}}_{\mathrm{O}_2}\right)x + \left(b^{\mathrm{XC}}_{\mathrm{RuO}_x} - b^{\mathrm{exp}}_{\mathrm{RuO}_x}\right) \quad (7)$$

Again, $\varepsilon^{\mathrm{XC}}_{\mathrm{RuO}_x}$ scales with a positive slope with x if $\left|m^{\mathrm{XC}}_{\mathrm{RuO}_x} + \frac{1}{2}\varepsilon^{\mathrm{XC}}_{\mathrm{O}_2}\right| < \left|m^{\mathrm{exp}}_{\mathrm{RuO}_x}\right|$.

3.3 Mitigating gas-phase errors

Fig. 3 shows that the uncorrected formation energies entail large deviations from experimental values for all functionals. The trends in Fig. 3a have similar slopes of ~−0.20 eV per O atom except for RPBE, which is nearly flat (0.04 eV per O atom). Meanwhile, hybrids exhibit an average slope of ~0.66 ± 0.10 eV per O atom in Fig. 3c.

In Fig. 3b and d, correcting $\varepsilon^{\mathrm{XC}}_{\mathrm{O}_2}$ makes all GGAs and meta-GGAs display similar slopes of −0.46 ± 0.15 eV per O atom. For the hybrids, the average slope is now 0.59 ± 0.04 eV per O atom. As the oxygen error does not affect $Ru_{(g)}$, the intercepts remain unchanged in Fig. 3b and d compared to those in Fig. 3a and c. Capitalizing on the linear trends in Fig. 3b and d provided by the inexpensive structural descriptor x, a corrected DFT free energy ($\Delta_f G^{\mathrm{XC,corr}}_{\mathrm{RuO}_x}$) can be obtained:[66]

$$\Delta_f G^{\mathrm{XC,corr}}_{\mathrm{RuO}_x} = \left(\Delta_f G^{\mathrm{XC}}_{\mathrm{RuO}_x} + \frac{x}{2}\varepsilon^{\mathrm{XC}}_{\mathrm{O}_2}\right) - \left(\delta^{\mathrm{XC}}x + \theta^{\mathrm{XC}}\right) \quad (8)$$

where δ^{XC} and θ^{XC} are the functional-dependent slope and intercept of the trends correlating $\varepsilon^{\mathrm{XC}}_{\mathrm{RuO}_x}$ *vs.* x. In Table 1, we report such slopes and intercepts for all scrutinized functionals. We note that $\varepsilon^{\mathrm{XC}}_{\mathrm{res}} = \Delta_f G^{\mathrm{XC,corr}}_{\mathrm{RuO}_x} - \Delta_f G^{\mathrm{exp}}_{\mathrm{RuO}_x}$ is a residual error stemming from the slight deviations of the calculated datapoints and the linear fits in Fig. 2. Such residual errors are shown for all functionals in Fig. 4, where we observe unsystematic, flat trends around 0 eV with mean and maximum

Table 1 Slopes (δ^{XC}) and offsets (θ^{XC}) of the lines correlating $\varepsilon^{\mathrm{XC}}_{\mathrm{RuO}_{x(g)}}$ and x for all functionals under study. All values are in eV

Functional	PBE	PW91	RPBE	SCAN	TPSS	R2SCAN	PBE0	HSEsol	HSE06
δ^{XC}	−0.39	−0.43	−0.34	−0.47	−0.75	−0.39	0.61	0.54	0.61
θ^{XC}	−0.07	0.08	−0.83	−0.08	0.15	−0.35	−1.83	−1.00	−1.75

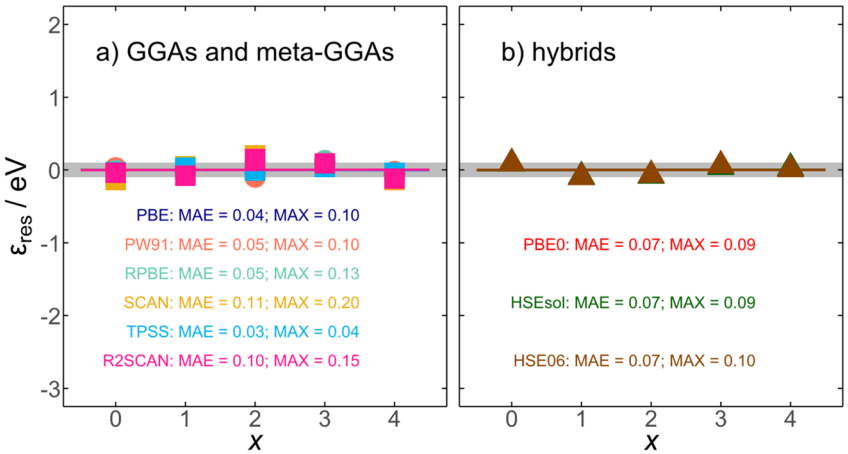

Fig. 4 Residual errors (ε_{res}) obtained after correcting the DFT formation energies using eqn (8). Results are shown for (a) GGAs and meta-GGAs (circles and squares, respectively) and (b) hybrid functionals (triangles). The gray region spans ±0.1 eV around zero. The final MAE/MAX values (in eV) are reported for all scrutinized functionals.

absolute errors (MAE and MAX) close to chemical accuracy (~0.04 eV). For instance, the uncorrected SCAN energy of formation for $RuO_{4(g)}$ entails an initial error of −2.12 eV, and after correcting with eqn (8), the residual error is only −0.14 eV.

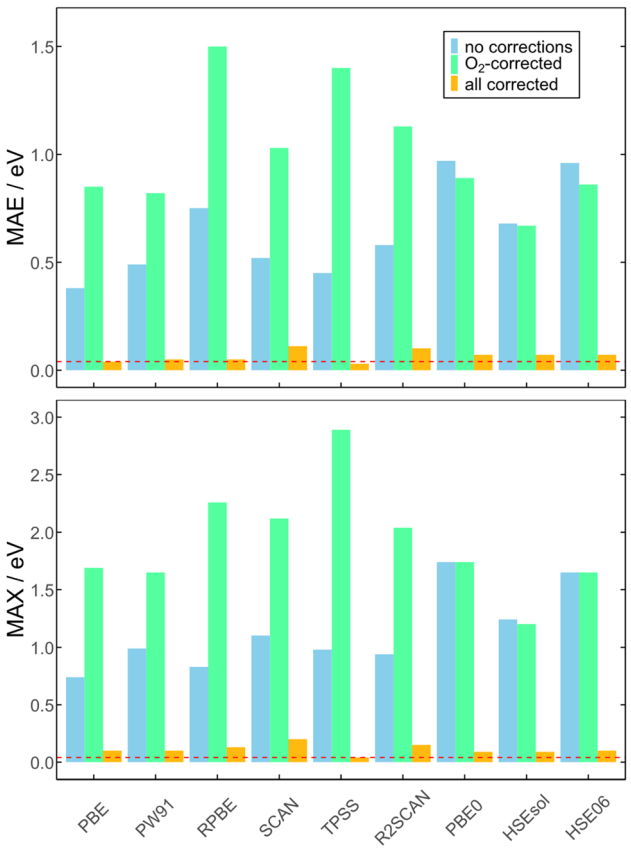

Fig. 5 (a) Mean absolute error (MAE) and (b) maximum absolute error (MAX) for different functionals when no gas-phase corrections are applied (blue), when only the $O_{2(g)}$ energy is corrected (green), and when $O_{2(g)}$ and RuO_x are corrected using eqn (8) and Table 1 (orange). The red dashed lines mark the chemical accuracy (1 kcal mol^{-1} ≈ 0.04 eV).

In addition, the average of the MAEs is 0.06 eV and the average of the MAXs is 0.11 eV. In sum, Fig. 4 attests to the removal of the systematic errors in RuO_x observed in Fig. 3 by means of simple linear corrections based on the number of oxygen atoms in the oxide.

Fig. 5 summarizes the MAEs and MAXs when no corrections are applied, when $O_{2(g)}$ is corrected, and when $O_{2(g)}$ and the oxides are corrected using eqn (8). A noteworthy feature of Fig. 5 is that both MAE and MAX values increase after correcting $O_{2(g)}$ for all GGAs and meta-GGAs, reaching MAE/MAX of 1.5/2.9 eV, while hybrids show a slight improvement. Finally, mitigating the errors using eqn (8) leads to the orange data in Fig. 5a and b, which are remarkably close to the red dashed line marking chemical accuracy. In fact, the largest final MAE and MAX (0.11 and 0.20 eV, respectively) are in stark contrast with the largest initial MAE and MAX (1.5 and 2.9 eV, respectively), illustrating that the corrections based on x swiftly and inexpensively lower the substantial DFT errors to the scale of chemical accuracy for all functionals.

3.4 Solid-phase errors

In the previous sections, large gas-phase errors in the DFT-calculated energies of RuO_x were unveiled, suggesting substantial deviations in reactions involving them. Although the analysis has focused so far on molecules, eqn (3) is also valid for solids. Bearing in mind that $\Delta_f G^{exp}_{RuO_{2(s)}} = -2.66$ eV,[52] the functional-dependent error $\varepsilon^{XC}_{RuO_{2(s)}}$ was estimated using eqn (3), as shown in Table S4.† Furthermore, Fig. S1† shows a comparison against its gaseous counterpart ($\varepsilon^{XC}_{RuO_{2(g)}}$). Encouragingly, the solid phase is better described than the gas phase; we did not observe any correlation between gas-phase and solid-state errors, and only for the meta-GGAs the magnitude of the solid-state error exceeds 0.3 eV. Indeed, the mean absolute values of $\varepsilon^{XC}_{RuO_{2(g)}}$ and $\varepsilon^{XC}_{RuO_{2(s)}}$ calculated from Tables S3 and S4† are significantly different in all cases: 1.08 *vs.* 0.16 eV for GGAs, 1.06 *vs.* 0.82 eV for meta-GGAs, and 0.43 *vs.* 0.24 eV for hybrid functionals.

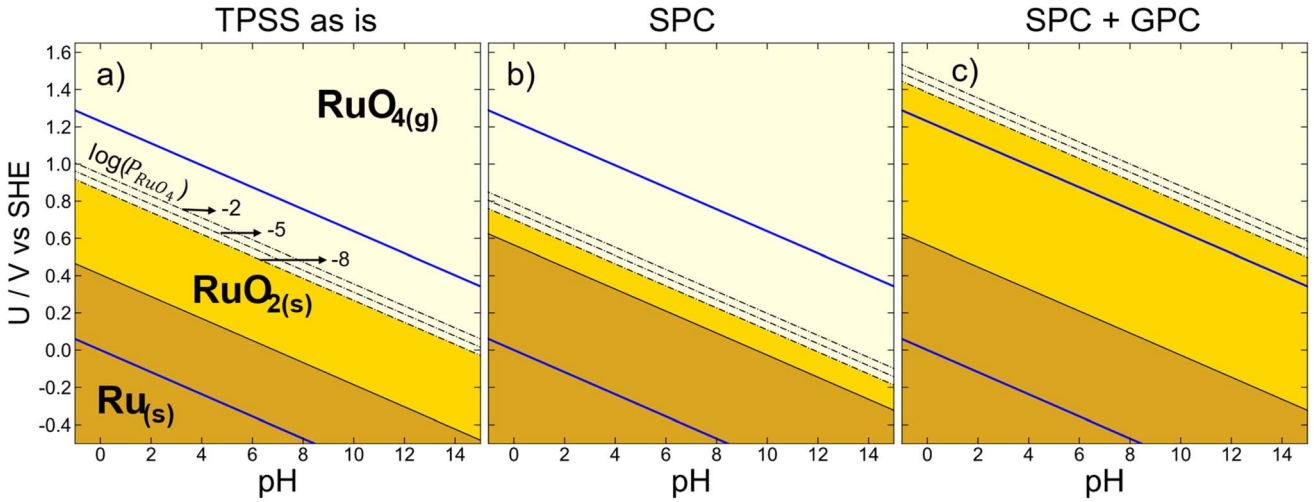

Fig. 6 TPSS-calculated Pourbaix diagram for the Ru–water system showing the stability regions of $Ru_{(s)}$, $RuO_{2(s)}$ and $RuO_{4(g)}$ as a function of the potential U (V *vs.* SHE) and pH. (a) Uncorrected TPSS energies ("TPSS as is"), (b) TPSS plus solid-phase corrections for $RuO_{2(s)}$ ("SPC"). (c) TPSS plus solid-state corrections for $RuO_{2(s)}$ and gas-phase corrections for $RuO_{4(g)}$ ("SPC + GPC"). The black dashed lines correspond to three different concentrations of $RuO_{4(g)}$ marked by $\log(P_{RuO_{4(g)}}) = -2$, -5, and -8. The blue lines show the upper and lower limits of water stability. The stability region of $Ru_{(s)}$ appears in dark orange, that of $RuO_{2(s)}$ in yellow, and that of $RuO_{4(g)}$ in beige.

3.5 Impact on electrochemistry

Stability and durability are necessary features of the materials used in electrochemical and electrocatalytic applications.[67–70] Pourbaix diagrams are useful to assess the thermodynamic stability of materials in aqueous media as a function of potential and pH, allowing to anticipate regions of protection, passivation and corrosion.[35] Importantly, as bulk and surface Pourbaix diagrams can be built entirely from DFT calculations,[71–74] it is crucial to appraise the DFT errors and uncertainty if an accurate picture of stable phases under reaction conditions is sought after.[75]

Below we illustrate the repercussions of DFT errors on the bulk Pourbaix diagram of the Ru–water system, considering the oxidations from $Ru_{(s)}$ to $RuO_{2(s)}$ and $RuO_{4(g)}$. This outlines a stability region for $RuO_{2(s)}$, which deserves special attention due to the negative impact of its dissolution to $RuO_{4(aq)}$ on the durability and catalytic performance for the OER.[31,76–78] Importantly, the degradation pathway involves compounds in the gas and solid phases, such that different sorts of DFT errors should be simultaneously addressed. Because Fig. 3a and b hinted toward particularly large meta-GGA errors in the energies of $RuO_{4(g)}$ and $RuO_{2(g)}$, TPSS is used as a case study.

In Fig. 6, the TPSS-based Pourbaix diagram for the Ru–water system is shown at three correction stages: in Fig. 6a no corrections are taken into account, in Fig. 6b only the solid-phase correction of $RuO_{2(s)}$ is considered, and Fig. 6c includes both the solid-phase and gas-phase corrections of $RuO_{2(s)}$ and $RuO_{4(g)}$. We recall that the errors of $RuO_{2(s)}$ and $RuO_{4(g)}$ result upon correcting the energy of $O_{2(g)}$ in their formation reactions (eqn (1)). The three scenarios depict contrasting regions, so whether and how many DFT errors are included can lead to different conclusions. For instance, the "TPSS as is" region of $Ru_{(s)}$ is smaller than when solid-phase and/or gas-phase corrections are added, so uncorrected $Ru_{(s)}$ oxidation is not accurately predicted.

The solid-phase correction shortens the $RuO_{2(s)}$ region in Fig. 6b, so that its vertical span is 0.10 V, in contrast to the 0.46 V in Fig. 6a. When the gas-phase energy of $RuO_{4(g)}$ is also corrected, the $RuO_{4(g)}$ region is shifted upwards such that the $RuO_{2(s)}$ phase has now a vertical width of 0.82 V, as shown in Fig. 6c. To incorporate pressure effects in the gas phase, the dashed lines in Fig. 6 mark three different partial pressures of $RuO_{4(g)}$ ($\log(P_{RuO_{4(g)}}) = -2$, -5, and -8). Besides, the blue lines delimit the water stability region in between $O_{2(g)}$ and $H_{2(g)}$ evolution. Table S10† contains the equilibrium potentials at the three correction stages in Fig. 6 for all functionals under study.

We close this section by stressing that additional phases can and ought to be included to enrich Fig. 6, whether they are gases, solids or aqueous species. In doing so, it is always advisable to properly assess the DFT errors since not only free molecules but also solids might be problematic.

4. Conclusions

DFT is widely employed to understand and improve the electrocatalytic performance of Ru-based electrodes, which display high activities for the CER and OER. Therefore, a proper description of the thermochemistry of Ru oxides is crucial to yield accurate predictions.

In this study, we analyzed the DFT-calculated free energies of formation for several Ru oxides using various GGA, meta-GGA and hybrid functionals. The gas-phase errors are substantial and increase linearly with the number of oxygen atoms in the compounds. The slopes of GGAs and meta-GGAs are negative and around -0.46 eV per O atom, while those of hybrids are positive and close to 0.59 eV per O atom. We elaborated an energy-decomposition model that explains (i) the linear relationship between the number of oxygen atoms and the formation energies of Ru oxides and (ii) the positive and negative slopes of the error trends.

We capitalized on the systematicity of the errors to provide a swift and inexpensive correction scheme that lowers the absolute errors to values close to chemical accuracy. In addition, $RuO_{2(s)}$ errors were computed and found to be smaller than their gas-phase counterparts, displaying absolute values of ~0.2 eV, except for the meta-GGAs for which the errors are larger than 0.6 eV.

Finally, the effects of solid-state and gas-phase DFT errors of RuO_x on electrochemical stability were appraised by means of bulk Pourbaix diagrams including $Ru_{(s)}$, $RuO_{2(s)}$, and $RuO_{4(g)}$ phases. The resulting Pourbaix diagrams showed that uncorrected or partially corrected TPSS energies produce reshaped regions visibly deviating from the fully corrected picture. In fact, the stability region of $RuO_{2(s)}$ is underestimated if solids and molecules are not corrected.

All in all, relying on DFT without being aware of its inaccuracies might lead to faulty models of chemical, electrochemical and catalytic reactions involving Ru oxides. This work provides a rational, inexpensive and semiempirical scheme to detect and quantify such errors and align predictions with experiments. Finally, this work can be used in future studies as a starting point to unveil similar trends for other families of oxidized electrocatalysts and enhance their DFT modelling.

Data availability

The data supporting this article have been included as part of the ESI.†

Conflicts of interest

The authors declare no conflicts of interest.

Acknowledgements

This work received financial support from grants PID2021-127957NB-I00 and TED2021-132550B-C21, which are funded by the Spanish MCIN/AEI/10.13039/501100011033 and the European Social Fund Plus (ESF+). The project that gave rise to these results also received the support of a Ph.D. fellowship from "la Caixa" Foundation (ID 100010434, fellowship code LCF/BQ/DI22/11940040). FCV also acknowledges financial support through grant IT1453-22 "Grupos Consolidados UPV/EHU del Gobierno Vasco". IAR thanks the Spanish MCIN for an FPI grant (PRE2022-103431). The use of supercomputing facilities at SURFsara was sponsored by NWO Physical Sciences, with financial support from NWO. We thank the Red Española de Supercomputación for providing computational resources through grants QHS-2025-1-0024, QHS-2024-3-0037 and QHS-2024-3-0025.

References

1 F. Miradji, S. Souvi, L. Cantrel, F. Louis and V. Vallet, Thermodynamic Properties of Gaseous Ruthenium Species, *J. Phys. Chem. A*, 2015, **119**(20), 4961–4971, DOI: **10.1021/acs.jpca.5b01645**.

2 C. Mun, L. Cantrel and C. Madic, Review of Literature on Ruthenium Behavior in Nuclear Power Plant Severe Accidents, *Nucl. Technol.*, 2006, **156**(3), 332–346, DOI: **10.13182/NT156-332**.

3 K. Iwanaga, K. Seki, T. Hibi, K. Issoh, T. Suzuta, M. Nakada, Y. Mori and T. Abe, *The Development of Improved Hydrogen Chloride Oxidation Process*, R&D Report, Sumitomo Kagaku, 2004.

4 S. Trasatti, Electrocatalysis: Understanding the Success of DSA®, *Electrochim. Acta*, 2000, **45**(15–16), 2377–2385, DOI: **10.1016/S0013-4686(00)00338-8**.

5 S. Trasatti and G. Buzzanca, Ruthenium Dioxide: A New Interesting Electrode Material. Solid State Structure and Electrochemical Behaviour, *J. Electroanal. Chem. Interfacial Electrochem.*, 1971, **29**(2), A1–A5, DOI: **10.1016/S0022-0728(71)80111-0**.

6 Y. Matsumoto and E. Sato, Electrocatalytic Properties of Transition Metal Oxides for Oxygen Evolution Reaction, *Mater. Chem. Phys.*, 1986, **14**(5), 397–426, DOI: **10.1016/0254-0584(86)90045-3**.

7 S. Trasatti, Electrocatalysis in the Anodic Evolution of Oxygen and Chlorine, *Electrochim. Acta*, 1984, **29**(11), 1503–1512, DOI: **10.1016/0013-4686(84)85004-5**.

8 R. K. B. Karlsson and A. Cornell, Selectivity between Oxygen and Chlorine Evolution in the Chlor-Alkali and Chlorate Processes, *Chem. Rev.*, 2016, **116**(5), 2982–3028, DOI: **10.1021/acs.chemrev.5b00389**.

9 W. T. Hong, M. Risch, K. A. Stoerzinger, A. Grimaud, J. Suntivich and Y. Shao-Horn, Toward the Rational Design of Non-Precious Transition Metal Oxides for Oxygen Electrocatalysis, *Energy Environ. Sci.*, 2015, **8**(5), 1404–1427, DOI: **10.1039/C4EE03869J**.

10 Y. Liu, Y. Wang and S. Zhao, Journey of Electrochemical Chlorine Production: From Brine to Seawater, *Curr. Opin. Electrochem.*, 2023, **37**, 101202, DOI: **10.1016/j.coelec.2022.101202**.

11 D. Crihan, M. Knapp, S. Zweidinger, E. Lundgren, C. J. Weststrate, J. N. Andersen, A. P. Seitsonen and H. Over, Stable Deacon Process for HCl Oxidation over RuO_2, *Angew. Chem., Int. Ed.*, 2008, **47**(11), 2131–2134, DOI: **10.1002/anie.200705124**.

12 P. C. K. Vesborg and T. F. Jaramillo, Addressing the Terawatt Challenge: Scalability in the Supply of Chemical Elements for Renewable Energy, *RSC Adv.*, 2012, **2**(21), 7933, DOI: **10.1039/c2ra20839c**.

13 K. A. Stoerzinger, O. Diaz-Morales, M. Kolb, R. R. Rao, R. Frydendal, L. Qiao, X. R. Wang, N. B. Halck, J. Rossmeisl, H. A. Hansen, T. Vegge, I. E. L. Stephens, M. T. M. Koper and Y. Shao-Horn, Orientation-Dependent Oxygen Evolution on RuO_2 without Lattice Exchange, *ACS Energy Lett.*, 2017, **2**(4), 876–881, DOI: **10.1021/acsenergylett.7b00135**.

14 Y. Qin, T. Yu, S. Deng, X.-Y. Zhou, D. Lin, Q. Zhang, Z. Jin, D. Zhang, Y.-B. He, H.-J. Qiu, L. He, F. Kang, K. Li and T.-Y. Zhang, RuO_2 Electronic Structure and Lattice Strain Dual Engineering for Enhanced Acidic Oxygen Evolution

Reaction Performance, *Nat. Commun.*, 2022, **13**(1), 3784, DOI: 10.1038/s41467-022-31468-0.
15 Z. Xu and J. R. Kitchin, Tuning Oxide Activity through Modification of the Crystal and Electronic Structure: From Strain to Potential Polymorphs, *Phys. Chem. Chem. Phys.*, 2015, **17**(43), 28943–28949, DOI: 10.1039/C5CP04840K.
16 H. Sun and W. Jung, Recent Advances in Doped Ruthenium Oxides as High-Efficiency Electrocatalysts for the Oxygen Evolution Reaction, *J. Mater. Chem. A*, 2021, **9**(28), 15506–15521, DOI: 10.1039/D1TA03452A.
17 N. B. Halck, V. Petrykin, P. Krtil and J. Rossmeisl, Beyond the Volcano Limitations in Electrocatalysis – Oxygen Evolution Reaction, *Phys. Chem. Chem. Phys.*, 2014, **16**(27), 13682–13688, DOI: 10.1039/C4CP00571F.
18 Z. W. Seh, J. Kibsgaard, C. F. Dickens, I. Chorkendorff, J. K. Nørskov and T. F. Jaramillo, Combining Theory and Experiment in Electrocatalysis: Insights into Materials Design, *Science*, 2017, **355**(6321), eaad4998, DOI: 10.1126/science.aad4998.
19 X. Liao, R. Lu, L. Xia, Q. Liu, H. Wang, K. Zhao, Z. Wang and Y. Zhao, Density Functional Theory for Electrocatalysis, *Energy Environ. Mater.*, 2022, **5**(1), 157–185, DOI: 10.1002/eem2.12204.
20 R. R. Rao, M. J. Kolb, N. B. Halck, A. F. Pedersen, A. Mehta, H. You, K. A. Stoerzinger, Z. Feng, H. A. Hansen, H. Zhou, L. Giordano, J. Rossmeisl, T. Vegge, I. Chorkendorff, I. E. L. Stephens and Y. Shao-Horn, Towards Identifying the Active Sites on RuO_2 (110) in Catalyzing Oxygen Evolution, *Energy Environ. Sci.*, 2017, **10**(12), 2626–2637, DOI: 10.1039/C7EE02307C.
21 J. K. Nørskov, J. Rossmeisl, A. Logadottir, L. Lindqvist, J. R. Kitchin, T. Bligaard and H. Jónsson, Origin of the Overpotential for Oxygen Reduction at a Fuel-Cell Cathode, *J. Phys. Chem. B*, 2004, **108**(46), 17886–17892, DOI: 10.1021/jp047349j.
22 J. I. Martínez, H. A. Hansen, J. Rossmeisl and J. K. Nørskov, Formation Energies of Rutile Metal Dioxides Using Density Functional Theory, *Phys. Rev. B: Condens. Matter Mater. Phys.*, 2009, **79**(4), 045120, DOI: 10.1103/PhysRevB.79.045120.
23 L. Wang, T. Maxisch and G. Ceder, Oxidation Energies of Transition Metal Oxides within the GGA + U Framework, *Phys. Rev. B: Condens. Matter Mater. Phys.*, 2006, **73**(19), 195107, DOI: 10.1103/PhysRevB.73.195107.
24 R. Christensen, H. A. Hansen, C. F. Dickens, J. K. Nørskov and T. Vegge, Functional Independent Scaling Relation for ORR/OER Catalysts, *J. Phys. Chem. C*, 2016, **120**(43), 24910–24916, DOI: 10.1021/acs.jpcc.6b09141.
25 E. Sargeant, F. Illas, P. Rodríguez and F. Calle-Vallejo, Importance of the Gas-Phase Error Correction for O_2 When Using DFT to Model the Oxygen Reduction and Evolution Reactions, *J. Electroanal. Chem.*, 2021, **896**, 115178, DOI: 10.1016/j.jelechem.2021.115178.
26 F. Calle-Vallejo, J. I. Martínez, J. M. García-Lastra, M. Mogensen and J. Rossmeisl, Trends in Stability of Perovskite Oxides, *Angew. Chem., Int. Ed.*, 2010, **49**(42), 7699–7701, DOI: 10.1002/anie.201002301.
27 R. Urrego-Ortiz, S. Builes, F. Illas and F. Calle-Vallejo, Gas-Phase Errors in Computational Electrocatalysis: A Review, *EES Catal.*, 2024, **2**(1), 157–179, DOI: 10.1039/D3EY00126A.
28 I. C. Man, H. Su, F. Calle-Vallejo, H. A. Hansen, J. I. Martínez, N. G. Inoglu, J. Kitchin, T. F. Jaramillo, J. K. Nørskov and J. Rossmeisl, Universality in Oxygen Evolution Electrocatalysis on Oxide Surfaces, *ChemCatChem*, 2011, **3**(7), 1159–1165, DOI: 10.1002/cctc.201000397.
29 L. G. V. Briquet, M. Sarwar, J. Mugo, G. Jones and F. Calle-Vallejo, A New Type of Scaling Relations to Assess the Accuracy of Computational Predictions of Catalytic Activities Applied to the Oxygen Evolution Reaction, *ChemCatChem*, 2017, **9**(7), 1261–1268, DOI: 10.1002/cctc.201601662.
30 Z. Xu, J. Rossmeisl and J. R. Kitchin, A Linear Response DFT+*U* Study of Trends in the Oxygen Evolution Activity of Transition Metal Rutile Dioxides, *J. Phys. Chem. C*, 2015, **119**(9), 4827–4833, DOI: 10.1021/jp511426q.
31 C. F. Dickens and J. K. Nørskov, A Theoretical Investigation into the Role of Surface Defects for Oxygen Evolution on RuO_2, *J. Phys. Chem. C*, 2017, **121**(34), 18516–18524, DOI: 10.1021/acs.jpcc.7b03481.
32 F. Studt, F. Abild-Pedersen, H. A. Hansen, I. C. Man, J. Rossmeisl and T. Bligaard, Volcano Relation for the Deacon Process over Transition-Metal Oxides, *ChemCatChem*, 2010, **2**(1), 98–102, DOI: 10.1002/cctc.200900194.
33 K. Klyukin, A. Zagalskaya and V. Alexandrov, Role of Dissolution Intermediates in Promoting Oxygen Evolution Reaction at RuO_2 (110) Surface, *J. Phys. Chem. C*, 2019, **123**(36), 22151–22157, DOI: 10.1021/acs.jpcc.9b03418.
34 A. Zagalskaya and V. Alexandrov, Role of Defects in the Interplay between Adsorbate Evolving and Lattice Oxygen Mechanisms of the Oxygen Evolution Reaction in RuO_2 and IrO_2, *ACS Catal.*, 2020, **10**(6), 3650–3657, DOI: 10.1021/acscatal.9b05544.
35 M. Pourbaix, *Atlas of Electrochemical Equilibria in Aqueous Solutions*, National Association of Corrosion Engineers, Houston, Texas, 2nd edn, 1974.
36 G. Kresse and J. Furthmüller, Efficient Iterative Schemes for Ab Initio Total-Energy Calculations Using a Plane-Wave Basis Set, *Phys. Rev. B: Condens. Matter Mater. Phys.*, 1996, **54**(16), 11169–11186, DOI: 10.1103/PhysRevB.54.11169.
37 G. Kresse and D. Joubert, From Ultrasoft Pseudopotentials to the Projector Augmented-Wave Method, *Phys. Rev. B: Condens. Matter Mater. Phys.*, 1999, **59**(3), 1758–1775, DOI: 10.1103/PhysRevB.59.1758.
38 J. P. Perdew, K. Burke and M. Ernzerhof, Generalized Gradient Approximation Made Simple [Phys. Rev. Lett. 77, 3865 (1996)], *Phys. Rev. Lett.*, 1997, **78**(7), 1396, DOI: 10.1103/PhysRevLett.78.1396.
39 J. P. Perdew and Y. Wang, Accurate and Simple Analytic Representation of the Electron-Gas Correlation Energy, *Phys. Rev. B: Condens. Matter Mater. Phys.*, 1992, **45**(23), 13244–13249, DOI: 10.1103/PhysRevB.45.13244.
40 B. Hammer, L. B. Hansen and J. K. Nørskov, Improved Adsorption Energetics within Density-Functional Theory

Using Revised Perdew-Burke-Ernzerhof Functionals, *Phys. Rev. B: Condens. Matter Mater. Phys.*, 1999, **59**(11), 7413–7421, DOI: 10.1103/PhysRevB.59.7413.

41 J. Sun, M. Marsman, G. I. Csonka, A. Ruzsinszky, P. Hao, Y.-S. Kim, G. Kresse and J. P. Perdew, Self-Consistent Meta-Generalized Gradient Approximation within the Projector-Augmented-Wave Method, *Phys. Rev. B: Condens. Matter Mater. Phys.*, 2011, **84**(3), 035117, DOI: 10.1103/PhysRevB.84.035117.

42 J. Sun, A. Ruzsinszky and J. P. Perdew, Strongly Constrained and Appropriately Normed Semilocal Density Functional, *Phys. Rev. Lett.*, 2015, **115**(3), 036402, DOI: 10.1103/PhysRevLett.115.036402.

43 J. Tao, J. P. Perdew, V. N. Staroverov and G. E. Scuseria, Climbing the Density Functional Ladder: Nonempirical Meta-Generalized Gradient Approximation Designed for Molecules and Solids, *Phys. Rev. Lett.*, 2003, **91**(14), 146401, DOI: 10.1103/PhysRevLett.91.146401.

44 J. W. Furness, A. D. Kaplan, J. Ning, J. P. Perdew and J. Sun, Accurate and Numerically Efficient r2SCAN Meta-Generalized Gradient Approximation, *J. Phys. Chem. Lett.*, 2020, **11**(19), 8208–8215, DOI: 10.1021/acs.jpclett.0c02405.

45 J. P. Perdew, M. Ernzerhof and K. Burke, Rationale for Mixing Exact Exchange with Density Functional Approximations, *J. Chem. Phys.*, 1996, **105**(22), 9982–9985, DOI: 10.1063/1.472933.

46 L. Schimka, J. Harl and G. Kresse, Improved Hybrid Functional for Solids: The HSEsol Functional, *J. Chem. Phys.*, 2011, **134**(2), 024116, DOI: 10.1063/1.3524336.

47 J. Paier, M. Marsman, K. Hummer, G. Kresse, I. C. Gerber and J. G. Ángyán, Screened Hybrid Density Functionals Applied to Solids, *J. Chem. Phys.*, 2006, **124**(15), 154709, DOI: 10.1063/1.2187006.

48 H. J. Monkhorst and J. D. Pack, Special Points for Brillouin-Zone Integrations, *Phys. Rev. B*, 1976, **13**(12), 5188–5192, DOI: 10.1103/PhysRevB.13.5188.

49 M. Methfessel and A. T. Paxton, High-Precision Sampling for Brillouin-Zone Integration in Metals, *Phys. Rev. B: Condens. Matter Mater. Phys.*, 1989, **40**(6), 3616–3621, DOI: 10.1103/PhysRevB.40.3616.

50 W. M. Haynes, D. R. Lide and T. J. Bruno, *CRC Handbook of Chemistry and Physics*, CRC Press/Taylor and Francis, Boca Raton, FL, 97th edn, 2016, DOI: 10.1201/9781315380476.

51 I. Nuta, C. Chatillon, F.-Z. Roki and E. Fischer, Gaseous Phase above Ru–O System: A Thermodynamic Data Assessment, *Calphad*, 2021, **75**, 102329, DOI: 10.1016/j.calphad.2021.102329.

52 C. Chatillon, I. Nuta, F.-Z. Roki and E. Fischer, Chemical Thermodynamics of $RuO_{2(s)}$, *J. Nucl. Mater.*, 2018, **509**, 742–751, DOI: 10.1016/j.jnucmat.2018.05.060.

53 *NIST Standard Reference Database Number 69*, 2023, DOI: 10.18434/T4D303.

54 R. Urrego-Ortiz, S. Builes and F. Calle-Vallejo, Fast Correction of Errors in the DFT-Calculated Energies of Gaseous Nitrogen-Containing Species, *ChemCatChem*, 2021, **13**(10), 2508–2516, DOI: 10.1002/cctc.202100125.

55 M. O. Almeida, M. J. Kolb, M. R. V. Lanza, F. Illas and F. Calle-Vallejo, Gas-Phase Errors Affect DFT-Based Electrocatalysis Models of Oxygen Reduction to Hydrogen Peroxide, *ChemElectroChem*, 2022, **9**(12), e202200210, DOI: 10.1002/celc.202200210.

56 L. P. Granda-Marulanda, A. Rendón-Calle, S. Builes, F. Illas, M. T. M. Koper and F. Calle-Vallejo, A Semiempirical Method to Detect and Correct DFT-Based Gas-Phase Errors and Its Application in Electrocatalysis, *ACS Catal.*, 2020, **10**(12), 6900–6907, DOI: 10.1021/acscatal.0c01075.

57 R. Urrego-Ortiz, M. Almeida and F. Calle-Vallejo, Error Awareness in the Volcano Plots of Oxygen Electroreduction to Hydrogen Peroxide, *ChemSusChem*, 2024, e202400873, DOI: 10.1002/cssc.202400873.

58 S. Kurth, J. P. Perdew and P. Blaha, Molecular and Solid-State Tests of Density Functional Approximations: LSD, GGAs, and Meta-GGAs, *Int. J. Quantum Chem.*, 1999, **75**(4–5), 889–909, DOI: 10.1002/(SICI)1097-461X(1999)75:4/5<889::AID-QUA54>3.0.CO;2-8.

59 R. Urrego-Ortiz, S. Builes, F. Illas, S. T. Bromley, M. C. Figueiredo and F. Calle-Vallejo, Minimum Conditions for Accurate Modeling of Urea Production via Co-Electrolysis, *Commun. Chem.*, 2023, **6**(1), 1–10, DOI: 10.1038/s42004-023-00990-7.

60 R. Urrego-Ortiz, S. Builes and F. Calle-Vallejo, Impact of Intrinsic Density Functional Theory Errors on the Predictive Power of Nitrogen Cycle Electrocatalysis Models, *ACS Catal.*, 2022, **12**(8), 4784–4791, DOI: 10.1021/acscatal.1c05333.

61 A. A. Peterson, F. Abild-Pedersen, F. Studt, J. Rossmeisl and J. K. Nørskov, How Copper Catalyzes the Electroreduction of Carbon Dioxide into Hydrocarbon Fuels, *Energy Environ. Sci.*, 2010, **3**(9), 1311–1315, DOI: 10.1039/C0EE00071J.

62 R. Christensen, H. A. Hansen and T. Vegge, Identifying Systematic DFT Errors in Catalytic Reactions, *Catal. Sci. Technol.*, 2015, **5**(11), 4946–4949, DOI: 10.1039/C5CY01332A.

63 H. Umeyama and K. Morokuma, The Origin of Hydrogen Bonding. An Energy Decomposition Study, *J. Am. Chem. Soc.*, 1977, **99**(5), 1316–1332, DOI: 10.1021/ja00447a007.

64 C. Dupont, Y. Jugnet and D. Loffreda, Theoretical Evidence of PtSn Alloy Efficiency for CO Oxidation, *J. Am. Chem. Soc.*, 2006, **128**(28), 9129–9136, DOI: 10.1021/ja061303h.

65 F. Calle-Vallejo, P. Sautet and D. Loffreda, Understanding Adsorption-Induced Effects on Platinum Nanoparticles: An Energy-Decomposition Analysis, *J. Phys. Chem. Lett.*, 2014, **5**(18), 3120–3124, DOI: 10.1021/jz501263e.

66 R. Urrego-Ortiz, S. Builes and F. Calle-Vallejo, Automated versus Chemically Intuitive Deconvolution of Density Functional Theory (DFT)-Based Gas-Phase Errors in Nitrogen Compounds, *Ind. Eng. Chem. Res.*, 2022, **61**(36), 13375–13382, DOI: 10.1021/acs.iecr.2c02111.

67 J. Masa, C. Andronescu and W. Schuhmann, Electrocatalysis as the Nexus for Sustainable Renewable Energy: The Gordian Knot of Activity, Stability, and Selectivity, *Angew. Chem., Int. Ed.*, 2020, **59**(36), 15298–15312, DOI: 10.1002/anie.202007672.

68 S. Geiger, O. Kasian, M. Ledendecker, E. Pizzutilo, A. M. Mingers, W. T. Fu, O. Diaz-Morales, Z. Li, T. Oellers, L. Fruchter, A. Ludwig, K. J. J. Mayrhofer, M. T. M. Koper and S. Cherevko, The Stability Number as a Metric for Electrocatalyst Stability Benchmarking, *Nat. Catal.*, 2018, **1**(7), 508–515, DOI: 10.1038/s41929-018-0085-6.

69 N. Esfandiari, M. Aliofkhazraei, A. N. Colli, F. C. Walsh, S. Cherevko, L. A. Kibler, M. M. Elnagar, P. D. Lund, D. Zhang, S. Omanovic and J. Lee, Metal-Based Cathodes for Hydrogen Production by Alkaline Water Electrolysis: Review of Materials, Degradation Mechanism, and Durability Tests, *Prog. Mater. Sci.*, 2024, **144**, 101254, DOI: 10.1016/j.pmatsci.2024.101254.

70 T. Fuchs, V. Briega-Martos, J. Drnec, N. Stubb, I. Martens, F. Calle-Vallejo, D. A. Harrington, S. Cherevko and O. M. Magnussen, Anodic and Cathodic Platinum Dissolution Processes Involve Different Oxide Species, *Angew. Chem.*, 2023, **135**(34), e202304293, DOI: 10.1002/ange.202304293.

71 H. A. Hansen, J. Rossmeisl and J. K. Nørskov, Surface Pourbaix Diagrams and Oxygen Reduction Activity of Pt, Ag and Ni(111) Surfaces Studied by DFT, *Phys. Chem. Chem. Phys.*, 2008, **10**(25), 3722, DOI: 10.1039/b803956a.

72 Z. Wang, X. Guo, J. Montoya and J. K. Nørskov, Predicting Aqueous Stability of Solid with Computed Pourbaix Diagram Using SCAN Functional, *npj Comput. Mater.*, 2020, **6**(1), 160, DOI: 10.1038/s41524-020-00430-3.

73 K. S. Exner, J. Anton, T. Jacob and H. Over, Chlorine Evolution Reaction on RuO_2(110): Ab Initio Atomistic Thermodynamics Study - Pourbaix Diagrams, *Electrochim. Acta*, 2014, **120**, 460–466, DOI: 10.1016/j.electacta.2013.11.027.

74 T. Fuchs, J. Drnec, F. Calle-Vallejo, N. Stubb, D. J. S. Sandbeck, M. Ruge, S. Cherevko, D. A. Harrington and O. M. Magnussen, Structure Dependency of the Atomic-Scale Mechanisms of Platinum Electro-Oxidation and Dissolution, *Nat. Catal.*, 2020, **3**(9), 754–761, DOI: 10.1038/s41929-020-0497-y.

75 O. Vinogradova, D. Krishnamurthy, V. Pande and V. Viswanathan, Quantifying Confidence in DFT-Predicted Surface Pourbaix Diagrams of Transition-Metal Electrode–Electrolyte Interfaces, *Langmuir*, 2018, **34**(41), 12259–12269, DOI: 10.1021/acs.langmuir.8b02219.

76 S. Cherevko, S. Geiger, O. Kasian, N. Kulyk, J.-P. Grote, A. Savan, B. R. Shrestha, S. Merzlikin, B. Breitbach, A. Ludwig and K. J. J. Mayrhofer, Oxygen and Hydrogen Evolution Reactions on Ru, RuO_2, Ir, and IrO_2 Thin Film Electrodes in Acidic and Alkaline Electrolytes: A Comparative Study on Activity and Stability, *Catal. Today*, 2016, **262**, 170–180, DOI: 10.1016/j.cattod.2015.08.014.

77 C. Roy, R. R. Rao, K. A. Stoerzinger, J. Hwang, J. Rossmeisl, I. Chorkendorff, Y. Shao-Horn and I. E. L. Stephens, Trends in Activity and Dissolution on RuO_2 under Oxygen Evolution Conditions: Particles versus Well-Defined Extended Surfaces, *ACS Energy Lett.*, 2018, **3**(9), 2045–2051, DOI: 10.1021/acsenergylett.8b01178.

78 H. Tamura and C. Iwakura, Metal Oxide Anodes for Oxygen Evolution, *Int. J. Hydrogen Energy*, 1982, **7**(11), 857–865, DOI: 10.1016/0360-3199(82)90003-9.